Broadband plasmonic nanoantenna with an adjustable spectral response

Eren Seydi Ünlü, Rüştü Umut Tok, and Kürşat Şendur[*]

Faculty of Engineering and Natural Sciences
Sabancı University, Orhanlı - Tuzla, 34956, Istanbul, Turkey

[*]*sendur@sabanciuniv.edu*

Abstract: Six-particle and eight-particle common-gap plasmonic nanoantennas are utilized to obtain a broadband spectral response when illuminated with circular and elliptical polarization. Due to the insensitivity of dipole antennas to circular polarization, the resonant structures are brought together around the common-gap to expand the spectrum of the whole system. Their ability to focus light at different frequencies is demonstrated. The spectral response is manipulated by geometrical parameters and the strength of the spectral peaks is tailored through the ellipticity of the elliptically polarized light.

© 2011 Optical Society of America

OCIS codes: (240.6680) Surface plasmons; (250.5403) Plasmonics.

References and links

1. P. Bharadwaj, B. Deutsch, and L. Novotny, "Optical Antennas," Adv. Opt. Photon. **1,** 438 (2009).
2. C. Peng, "Surface-plasmon resonance of a planar lollipop near-field transducer," Appl. Phys. Lett. **94,** 171106 (2009).
3. K. Sendur, C. Peng, and W. Challener, "Near-field radiation from a ridge waveguide transducer in the vicinity of a solid immersion lens," Phys. Rev. Lett. **94,** 043901 (2005).
4. A. Hartschuh, E. J. Sánchez, X. S. Xie, and L. Novotny, "High-resolution near-field Raman microscopy of single-walled carbon nanotubes," Phys. Rev. Lett. **90,** 095503 (2003).
5. L. Wang and X. Xu, "Numerical study of optical nanolithography using nanoscale bow-tie-shaped nano-apertures," J. Microsc. **229,** 483–489 (2008).
6. H. Atwater and A. Polman, "Plasmonics for improved photovoltaic devices," Nat. Mater. **9,** 205 (2010).
7. D. K. Kotter, S. D. Novack, W. D. Slafer, and P. J. Pinhero, "Theory and manufacturing processes of solar nanoantenna electromagnetic collectors," J. Sol. Energ-T ASME **132,** 011014 (2010).
8. R. M. Bakker, V. P. Drachev, H.-K. Yuan, V. M. Shalaev, "Near-field, broadband optical spectroscopy of meta-materials," Physica B **394,** 137 (2007).
9. S. V. Boriskina and L. Dal Negro, "Multiple-wavelength plasmonic nanoantennas," Opt. Lett. **35,** 538 (2010).
10. P. Biagioni, J. S. Huang, L. Duò, M. Finazzi, and B. Hecht, "Cross resonant optical antenna," Phys. Rev. Lett. **102,** 256801, (2009).
11. K. Sendur, W. Challener, and C. Peng, "Ridge waveguide as a near-field aperture for high density data storage," J. Appl. Phys. **96,** 2743–2752 (2004).
12. E. D. Palik, *Handbook of optical constants of solids* (Academic Press, San Diego, CA, 1998).

Nanoscale metallic antennas couple incident optical beams to length scales much smaller than the diffraction limit at optical frequencies [1]. Effective coupling of incident optical energy around the antenna gap can be utilized in many potential applications including optical data storage [2], heat assisted magnetic recording [3], near-field imaging [4], and nanolithography [5]. The history, basic concepts and parameters associated with optical antennas, and potential applications are discussed in a recent review article [1].

Plasmonic structures have been utilized to improve the energy conversion efficiency of photovoltaic devices [6]. By embedding plasmonic particles in solar cells the absorption cross section and energy conversion efficiency have been increased [6]. Recently, nanoantennas have been utilized in solar cells as electromagnetic collectors to improve the conversion efficiency of the devices in the spectral regime where the majority of the solar energy is present [7]. A major challenge for plasmonic nanoantennas in solar cells is their narrow band spectral response. The spectrum of the incident solar radiation is broad, whereas, the spectrum of plasmonic nanostructures is narrow with sharp resonances. Plasmonic antennas with a broadband spectral response are an emerging need to improve the efficiency of photovoltaic devices. In addition, it is desirable to tailor the spectral response of the nanoantenna based on the needs of various other applications. Tightly localized broadband optical sources can also be utilized for spectroscopy. Near-field broadband optical spectroscopy of materials is of interest [8], since a broadband source can be utilized over a wide range of wavelengths simultaneously. As a result near-field images can be obtained within a broad spectral range in a single experiment.

In a recent study, Broskina and Dal Negro [9] proposed grating-assisted nanoantennas that provide multiwavelength focusing in a single subwavelength spot. The authors utilized multiple-periodic gratings of different periodicities. By embedding conventional dimer gaps in multiple-periodic gratings, the authors demonstrated that multiwavelength focusing can be achieved by tuning the periodicities of the gratings and particle radii. In addition, cross-dipole antennas [10] have been utilized to obtain localized fields of various polarizations.

In this study, we propose six-particle and eight-particle common-gap plasmonic nanoantennas to obtain a broadband spectral response when they are illuminated with circular and elliptic polarization. The antennas utilized in this study are illustrated in Fig. 1. The insensitivity of a dipole antenna to circular polarization is utilized to bring dipole antennas together around the common-gap to expand the spectrum of the whole system. Their ability to focus light at different frequencies is demonstrated in this study.

To analyze this problem, a 3-D frequency-domain finite element method is utilized [3, 11]. The accuracy of the solution technique was previously validated by comparison with other solution techniques [3, 11]. The total electric field $\vec{E}^t(\vec{r})$ is composed of the summation of two components $\vec{E}^i(\vec{r})$ and $\vec{E}^s(\vec{r})$. The incident field $\vec{E}^i(\vec{r})$ represents the optical beam in the absence of the nanoantenna. Once the incident field interacts with the nanoantenna, scattered fields $\vec{E}^s(\vec{r})$ are generated. In this study, the incident field is a plane wave. To obtain the scattered field $\vec{E}^s(\vec{r})$,
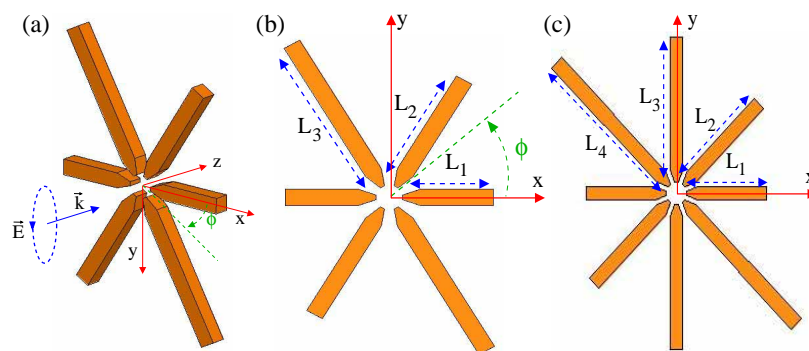

Fig. 1. (a) An oblique view of the six-particle common-gap plasmonic antenna, which is illuminated with a circularly polarized diffraction-limited incident beam propagating in the $\hat{z}$-direction. (b) Top view of the six-particle common-gap antenna composed of three dipole pairs with lengths L_1, L_2, and L_3. (c) Top view of the eight-particle common-gap antenna.

we used a 3-D finite element method (FEM) based full-wave solution of Maxwell's equations. To represent the scattering geometries accurately, tetrahedral elements are used to discretize the computational domain. In this study, the simulation domain is cubical. For the radiation boundary conditions, perfectly matched layers are utilized. The medium surrounding the antennas is air. On the tetrahedral elements, edge basis functions and second-order interpolation functions are used to expand the functions. Adaptive mesh refinement is used to improve the coarse solution regions with high field intensities and large field gradients. Once the scattered field is solved via FEM, the total field is obtained by adding the incident field to the scattered field. In this study, the dielectric constants of gold is chosen from the experimental data by Palik [12].

Six-particle and eight-particle broadband plasmonic antennas, composed of 3 or 4 pairs of elongated particles, are illustrated in Fig. 1. An oblique view of a six-particle antenna is given in Fig. 1(a). The spectral response of the broadband antennas depends on the spectral response of individual dipole antennas of which the size and spatial placement are carefully selected to tune the overall spectral response. The proposed antennas are illuminated with a circularly polarized incident beam, which plays an important role in expanding the bandwidth as discussed below.

The spectral response of a dipole antenna is sensitive to linear polarization. To excite a strong resonance on a dipole antenna by linear polarization, one has to illuminate the dipole antenna while the polarization is aligned with the long axis of the antenna. If the antenna is illuminated with a linearly polarized electric field perpendicular to the long-axis, then there will be no field enhancement in the gap region of the antenna. Figure 2(a) illustrates the sensitivity of the spectral response of a dipole antenna to linear polarization. The length, thickness, and width of the antenna are 100nm, 20 nm, and 20 nm, and the gap is 30 nm. The dipole antenna is illuminated with linearly polarized incident electromagnetic radiation, which can be expressed as

$$\vec{E} = \hat{x}\cos\left(\omega t - kz\right) \tag{1}$$

As shown in the inset of Fig. 2(a), a dipole antenna is oriented at an angle of ϕ with respect to the x-axis. When the antenna is aligned with the x-axis, i.e. $\phi=0$, the intensity is maximum as expected. As the angle ϕ is increased, the response of the nanoantenna drops sharply.
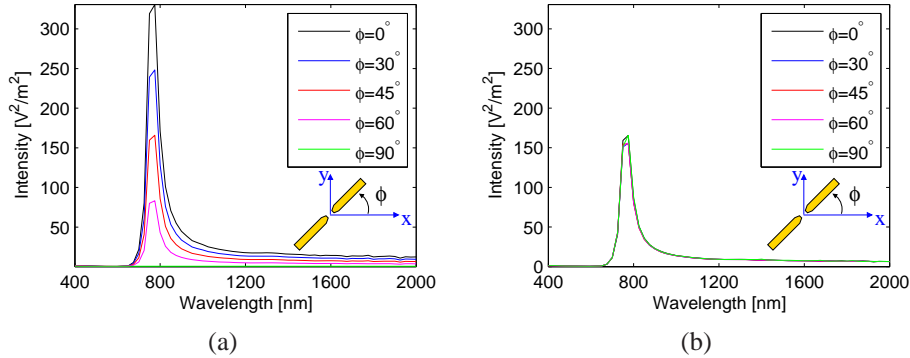

Fig. 2. Intensity distribution at the center of a nanoantenna as a function of orientation angle ϕ: (a) for linearly polarized light, (b) for circularly polarized light.

When a dipole antenna is illuminated with a circularly polarized beam, the antenna will respond to circularly polarization regardless of its orientation. The circularly polarized beam is given as

$$\vec{E} = \frac{\hat{x}}{\sqrt{2}}\cos\left(\omega t - kz\right) + \frac{\hat{y}}{\sqrt{2}}\sin\left(\omega t - kz\right) \tag{2}$$

where the amplitude is normalized to 1, similar to Eq. (1). As shown in Fig 2(b) it does not matter whether the long axis of the antenna is aligned with the $\hat{x}$-axis, $\hat{y}$-axis, or in between the $\hat{x}$-$\hat{y}$ axis since the incident beam is circularly symmetric. In other words, while a dipole antenna is rotationally sensitive to linear polarization, it is rotationally insensitive to circular polarization. Due to their insensitivity to circular polarization, the resonant structures can be brought together at the common-gap and the spectrum of the whole system can be expanded.

The resonances of the dipole antennas are very narrow as shown in Fig. 2. To address the narrow bandwidth of dipole antennas, the plasmonic antennas shown in Fig. 1 are used. Optical antennas with various lengths are studied, as listed in Table 1. Cases A to F correspond to six-particle antennas and Case G corresponds to an eight-particle antenna. The gap size is selected as 30 nm, which results in the neighboring particles not touching each other. The width and thickness of the antennas are both 20 nm. Each of the dipole antenna pairs in Fig. 1 resonate at different wavelengths. To achieve resonance of different pairs at different wavelengths, a circularly polarized beam of light is utilized since dipole antennas are rotationally insensitive to the circular polarization. The tip of the electric field vector for linearly polarized light sweeps a line as time progresses, therefore, it can not excite all the dipole pairs in Fig. 1. The tip of the electric field vector for circularly polarized light, on the other hand, sweeps a circle in time. Therefore, it can excite all three dipole pairs in Fig. 1.

Table 1. A list of nanoantenna lengths and corresponding FWHM

Case ID	L_1 [nm]	L_2 [nm]	L_3 [nm]	L_4 [nm]	FWHM [nm]
Case A	160	180	200	n/a	470
Case B	140	170	200	n/a	550
Case C	120	160	200	n/a	650
Case D	100	150	200	n/a	340
Case E	170	200	230	n/a	615
Case F	200	230	260	n/a	760
Case G	120	160	200	240	990

In Figs. 3(a) and (b), the spectral response of various antennas are presented when they are illuminated with the circularly polarization in Eq. (2). The FWHM of the spectral responses are listed in Table 1. Fig. 3(a) demonstrates how the spectral response is broadened and FWHM increases by increasing the variation between the antenna lengths. Fig. 3(b) demonstrates how the spectral response is shifted by changing the antenna lengths. For Cases A-C, the three spectra fall in the same width of the FWHM. When the length variation among antenna pairs is large, such as Case D, then the three spectra do not fall in the same width of the FWHM, reducing it. Fig. 3(c) illustrates that the spectral response can be further broadened by using an eight-particle antenna, for which the added pair increased the FWHM from 650 nm to 990 nm.

Multiple peaks observed in Figs. 3(a)-(c) are unique to circular polarization and the same results are not obtained with linear polarization. Figure 3(d) compares the results of the antenna in Case D when it is illuminated compared with circular polarization with 2 different linear polarizations. Figure 3(d) illustrates the spectral response for polarization angles $\phi = 0°$ and $\phi = 45°$. For $\phi = 0°$, the linear polarization expression was previously given by Eq. (1). The mathematical expression for the polarization angle $\phi = 45°$ case is given as

$$\vec{E} = \frac{\hat{x}}{\sqrt{2}} \cos\left(\omega t - kz\right) + \frac{\hat{y}}{\sqrt{2}} \cos\left(\omega t - kz\right) \tag{3}$$

The results in Fig. 3(d) shows that at most 2 peaks of the spectral resonance curve can be excited with linear polarizations in Eq. (1) and Eq. (3).
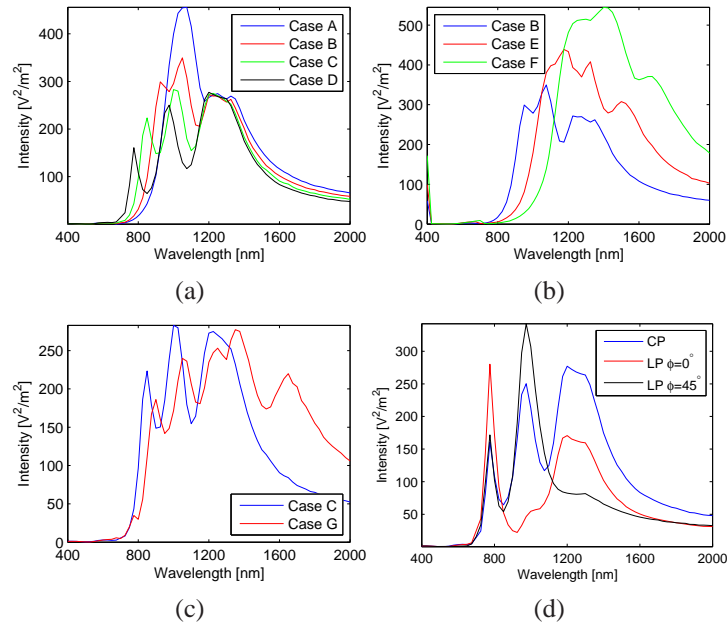
Fig. 3. Spectral response of various antennas illuminated with various polarizations. The electric field intensity at the center of the gap is plotted as a function of wavelength. (a) Spectral broadening by increasing the antenna length variation for circular polarization. (b) Spectral shifting with changing antenna lengths for circular polarization. (c) A comparison of six-particle and eight-particle antenna responses for circular polarization. (d) A comparison of a six-particle antenna, which is illuminated with circular polarization and two linearly polarizations given by Eq. (1) and Eq. (3).

An important aspect of the plasmonic antennas shown in Fig. 1 is their ability to focus light at different frequencies as illustrated in Fig. 4. The electric field distribution on the $\hat{x}$-$\hat{y}$ plane is plotted at various wavelengths for Case D. Figure 4(a) illustrates the electric field distribution at $\lambda = 400$ nm. Figure 4(a) shows a very weak intensity at the gap region of the antenna and none of the antenna components are at resonance. Figure 4(b) shows the field distribution that corresponds to the first spectral peak in Case D, i.e. at $\lambda = 775$ nm. A strong electric field distribution is observed in the gap region in Fig. 4(b). In addition, the horizontal oriented dipole shows a strong absorption profile, which is associated with the plasmon resonance of the dipole pair with the length $L_1 = 100$ nm. The electric field distributions that correspond to the second ($\lambda = 975$ nm) and third ($\lambda = 1200$ nm) spectral peaks in Case D are illustrated in Figs. 4(c) and 4(d), respectively. At these wavelengths, the dipole pairs indicated with lengths $L_2 = 150$ nm and $L_3 = 200$ nm resonate respectively, as shown in Figs. 4(c) and 4(d). Similar to other studies in the literature [9], the nanoantenna can focus light at different frequencies. The antenna in Fig. 1 may offer advantages, since it is a compact device with sizes on the order of a few hundred nanometers. In addition, the antenna in Fig. 1 can be easily integrated with different optical components, such as at the tip of a tapered fiber probe. For practical use of this antenna in a solar cell application, unpolarized radiation needs to be efficiently converted to various polarizations.

The strength of the spectral peaks is tailored through the ellipticity of elliptically polarized light. For example, for Case D in Fig. 3(a) the first peak is weaker than the other two peaks. This can be adjusted by using an elliptical polarized incident beam. By tuning the ellipticity of the incident elliptical polarization, the spectral distribution can be manipulated as shown in
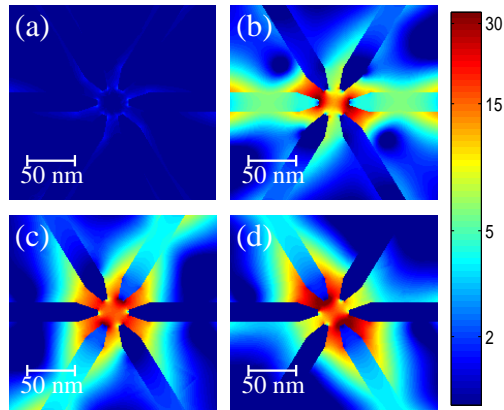
Fig. 4. Electric field intensity distribution on the $\hat{x}$-$\hat{y}$ plane: (a) at $\lambda = 400$ nm, which corresponds to off-resonance, (b) at $\lambda = 775$ nm, first spectral peak in Case D, (c) at $\lambda = 975$ nm, second spectral peak in Case D, and (d) at $\lambda = 1200$ nm, third spectral peak in Case D.
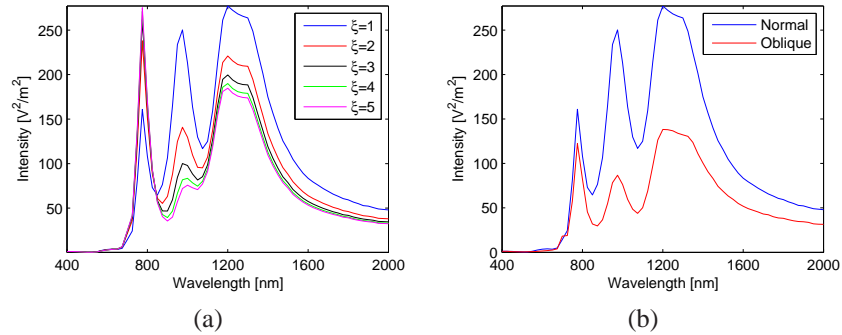

Fig. 5. (a) Spectral response of the antenna for elliptically polarization defined in Eq. (4). (b) A comparison of normal and oblique incidence for circular polarization.

Fig. 5(a). By using an elliptically polarized beam given as

$$\vec{E} = \hat{x} \frac{\xi}{\sqrt{\xi^2 + 1}} \cos\left(\omega t - kz\right) + \hat{y} \frac{1}{\sqrt{\xi^2 + 1}} \sin\left(\omega t - kz\right) \tag{4}$$

The relative amplitudes of the spectral peaks are adjusted by tuning the parameter ξ in Fig. 5(a). A similar effect can be obtained by using a circularly polarized beam at an oblique angle of $45°$ as shown in Fig. 5(b). At normal incidence, circular polarization traces a circle on the $\hat{x} - \hat{y}$ in time, of which the projection is an ellipse on the $\hat{x} - \hat{y}$ for oblique incidence.

In summary, a broadband spectral response was obtained from six-particle and eight-particle common-gap plasmonic nanoantennas for circular polarization excitation. It was demonstrated that the broadband plasmonic antenna is capable of focusing light at different frequencies over a large spectral band. In addition, it was demonstrated that the spectral distribution can be tailored using an elliptically polarized incident beam and by adjusting its ellipticity or circular polarization at an oblique incidence.

Acknowledgement